



Synthesis and Characterization of Zinc Oxide Nanoparticles Using *Cynara scolymus* Leaves: Enhanced Hemolytic, Antimicrobial, Antiproliferative, and Photocatalytic Activity

Mariappan Rajapriya¹ · Sundararaj Aruna Sharmili¹ · Raju Baskar² · Ravichandran Balaji³ · Naiyf S. Alharbi⁴ · Shine Kadaikunnan⁴ · Jamal M. Khaled⁴ · Khalid F. Alanzi⁴ · Baskaralingam Vaseeharan⁵

Received: 5 July 2019 / Published online: 3 October 2019
© Springer Science+Business Media, LLC, part of Springer Nature 2019

Abstract

Cynara scolymus leaves were used in the green synthesis of zinc oxide nanoparticles (ZnO NPs). ZnO NPs was confirmed by the formation of a white precipitate. UV–visible spectroscopy results showed a strong absorbance peak at 371 nm. The use of SEM confirmed the spherical shape of the nanoparticles, which had an average size of 65.9 nm. The nanoparticle zinc (80.17%) and oxygen (19.83%) composition was confirmed using energy-dispersive X-ray analysis (EDXA). X-ray power diffraction (XRD) spectra confirmed the crystalline nature of the nanoparticles. We found 0.5% hemolysis following the addition of 100 µg/ml of ZnO NPs. A MIC study found that bacteria were more susceptible to ZnO NPs relative to fungi. The ZnO NPs photocatalytic degradation activity was assessed using methyl violet and malachite green, which exhibited 94.3% degradation after 120 min of UV exposure and 89.5% degradation after 120 min of UV exposure, respectively. Using human breast cancer cell line (MCF 7) and Vero cells, we found half maximal IC₅₀ values of 65.31 µg/µl and 957.85 µg/µl, respectively, following antiproliferative assays. Thus, green synthesized ZnO NPs were found to possess hemolytic, antimicrobial, photocatalytic, and antiproliferative activities, and as such could be used in the development of novel drugs.

Keywords *Cynara scolymus* · ZnO NPs · SEM · XRD · Biological properties · Cancer cell line

✉ Sundararaj Aruna Sharmili
arsharmilis@gmail.com

✉ Baskaralingam Vaseeharan
vaseeharanb@gmail.com

¹ Department of Biotechnology, Stella Maris College (Autonomous), Chennai, Tamil Nadu 600 086, India

² Department of Biotechnology, University of Madras, Chennai, Tamil Nadu 600 025, India

³ Department of CAS Botany, University of Madras, Chennai, Tamil Nadu 600 025, India

⁴ Department of Botany and Microbiology, College of Science, King Saud University, Riyadh 11451, Saudi Arabia

⁵ Department of Animal Health and Management, Alagappa University, Science Block, 6th Floor, Burma Colony, Karaikudi, Tamil Nadu 630 004, India

Introduction

Nanotechnology primarily concerns the study of particles ranging from 1 to 100 nm in size [1]. An interdisciplinary field, Nanotechnology incorporates bionanoscience, materials science, and technology [2], and also relies heavily on the fields of biology, chemistry, and physics [3]. Nanoparticles are widely used in a range of applications owing to their optical, biological, and physiochemical properties [4–7].

Nanoparticles can be synthesized using physical, chemical, and biological methods [8, 9]. Biological nanoparticle synthesis typical involves the use of microorganisms, fungi, algae, and plants. The green synthesis method has recently become widely-used, as it allows the use of less toxic chemicals [1, 10] that are safe when released into the environment. Green-synthesized nanoparticles produced from plants are also more stable,

and synthesis by plants is faster relative to other methods of synthesis [4, 11].

Nanoparticles have a wider range of applications relative to larger particles as they have a much higher surface area to volume ratio, which allows them to more efficiently act as active components [8, 12]. Metal oxides typically form closely-packed structures and often exhibit antimicrobial, magnetic, and catalytic qualities [13]. Green-synthesized nanoparticles are highly compatible, and so they can be used in a number of biomedical and pharmaceutical applications [14]. ZnO NPs are widely used in the packaging of food [15] and in the production of paints and varnishes [8]. They also block harmful UV radiation, a quality which makes them valuable in the production of cosmetics and sunscreens [8].

Metal oxide nanoparticles possess catalytic qualities and as such are commonly used in the elimination of toxic hazardous chemical substances, primarily in the field of environmental safety [1]. The catalytic properties of ZnO NPs are due to their crystal structure, porosity, surface area, size distribution, and band gap, and are often used in photocatalytic degradation [9, 16]. Recently, number studies are reported on photocatalytic capacity of ZnO NPs [17–20].

Cynara scolymus L., commonly known as artichoke, is often used in the synthesis of Ag NPs. *C. scolymus* belongs to the family Asteraceae and originated in the Mediterranean, although it is now cultivated worldwide [21]. Artichoke has some medicinal value and is commonly used as a hepato-protectant. Artichoke leaf extract is also used in the treatment of hepatitis and hyperlipidemia in traditional European medicine. *C. scolymus* leaves and head extracts have been used in folk medicine as they have choleric and hepatoprotective activities there by enhancing the liver function. They are also used in the treatment of chronic liver and gall bladder diseases, hepatitis, jaundice, symptoms of diabetes and arteriosclerosis [22]. The active components present in the leaves of *C. scolymus* include luteolin, apigenin, glycosides, monocaffeoylquinic acids, dicaffeoylquinic acids, and sesquiterpenes [23]. Although, *C. scolymus* leaves contain up to 2% of phenolic acids (chlorogenic acid, cynarin and caffeic acid), 0.4% of bitter sesquiterpenes lactones (cynaropicrin, grosheimin), 0.1–1% flavonoids (luteolin such as scolymoside, cynaroside, apigenin-7-*O*-rutinoside, cynarasaponins, inulin) [24]. The leaf extracts of *C. scolymus* have antioxidative, antibacterial, anti-HIV, hepatoprotective, choleric activity apart from the ability to inhibit cholesterol biosynthesis and LDL oxidation [25]. Hence, the present study aimed to investigate the potential for ZnO NP synthesis using artichoke leaves. To our best knowledge this is a first report on ZnO NPs synthesis using artichoke leaves extract. An attempt was also made in this study to assess the particles'

hemolytic, antimicrobial, photocatalytic, and antiproliferative activity, to determine whether they can be effectively used as a drug.

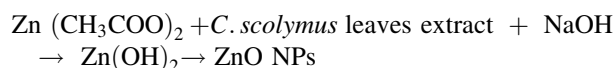
Materials and Methods

Preparation of Plant Samples

Artichoke leaves (*Cynara scolymus* L.) were collected from Ooty, The Nilgiris, Tamil Nadu, India. After collection, the artichoke leaves were dried and chopped into small pieces and divided into 10 g samples. The samples were added to 100 ml of distilled water and boiled at 100 °C for 10 min. The mixture was allowed to cool and then filtered using Whatmann filter paper No.1. The filtered extract was then stored at 4 °C for further use [15].

Synthesis of ZnO NPs

The ZnO NPs synthesis was achieved by co-precipitation method. To synthesis of ZnO NPs *C. scolymus* leaves extract were added drop by drop to the salt solution act as reducing capping and stabilizing agent. NaOH solution (2 M) was then added to adjust the pH to 12. The solution was kept on a heating magnetic stirrer and constantly stirred while the temperature was maintained at 100 °C. The resulting solution contained a white-colored precipitate, which confirmed the formation of ZnO NPs. The precipitate was separated by centrifugation at 10,000 rpm at 4 °C for 10 min. The resulting pellet was then washed with distilled water and ethanol. The pellet obtained was calcinated in a muffle furnace at 200 °C for 2 h. The white powdered ZnO NPs obtained were stored in vials for further use [26].



Characterization of ZnO NPs

UV-Spectrophotometry (Elico) was used to study the optical properties of the synthesized ZnO NPs. Readings were taken at wavelengths ranging from 250 to 400 nm. To identify the functional groups present in the ZnO NPs, FTIR was used between the ranges of 400–4000 cm^{-1} . To study the shape and size of the nanoparticles, SEM was used. Scanning was performed at magnifications ranging from 30,000 \times to 80,000 \times . The shape of the nanoparticles was again confirmed using TEM analysis (TEM-2100 plus electron microscope). The elemental composition of the ZnO NPs was determined using EDXA. The crystalline

nature and the size of the ZnO NPs were studied using XRD (Panalytical X'pert powder XRD system). The size of the ZnO NPs was determined using Debye–Scherrer's formula:

$$D_p = (0.94 \times \lambda) / (\beta \times \cos\theta)$$

where D_p is the average crystalline size, β is the line broadening in radians, θ is the Bragg's angle, and λ is the X-Ray wavelength (0.15418).

Hemolytic Activity

Fresh human blood samples (2 ml) (first author's blood sample) were collected and citrated to prevent coagulation. Samples were washed three times with phosphate buffer saline (pH 7.4) and centrifuged at 1000 rpm for 10 min. Red blood cells were obtained as a pellet and the supernatant-containing platelet-deficient plasma was discarded [27, 28]. The pellet was resuspended with 20 ml of PBS to create an equal suspension. The red blood cells were treated with an equal volume of ZnO NPs at concentrations ranging from 0.7 to 100 $\mu\text{g}/\mu\text{l}$. The samples were then incubated at 25 °C for 30 min. The positive control was prepared by adding 2% Triton X and the negative control contained cells treated with PBS only. Following incubation, the red blood cells were collected as a pellet by centrifugation at 5000 rpm for 5 min. The supernatant was utilized for subsequent absorbance studies [29]. Absorbances were read at 540 nm using a microplate reader (ELISA reader, Bio-rad). The percentage of hemolysis was calculated using the following formula:

$$\text{Hemolysis}(\%) = 100 \times (\text{OD test sample} - \text{OD PBS}) / (\text{OD Triton X} - \text{OD PBS})$$

Minimum Inhibitory Concentration

The green synthesized zinc oxide nanoparticles were checked for their antimicrobial activity using different of clinically important bacterial and fungal strains. These strains included *Staphylococcus aureus*, *Escherichia coli*, and *Pseudomonas aeruginosa* as well as *Candida albicans* and *Candida tropicalis*. Microbroth dilution assays were performed to find out the MIC of the synthesized nanoparticles for each taxon. Nutrient broth was used to culture bacteria and Sabraud dextrose broth was used to culture fungi. The test was carried out in a 96 well plate. One hundred microliters of the nutrient broth and Sabraud dextrose broth were placed in wells 2–10. Two hundred microliters of nanoparticles were added to these wells, which were then serially diluted. The inoculum (100 μl) was then added. The 11th well was used for the positive control

(media) and the 12th well was used for the negative control (inoculum). The plate was then sealed and incubated at 37 °C for 24 h. Absorbances were read at 490 nm on a microplate reader (ELISA reader) [30, 31]. MIC percentages were calculated using the following formula:

$$\text{Inhibition}(\%) = 1 - \text{OD of test} / \text{OD of control} \times 100$$

Photocatalytic Activity

Photocatalytic degradation assays were performed using methyl violet and malachite green. Each dye was prepared at a concentration of 10 ppm. The dyes (10 ml) were placed in separate test tubes and marked as a control. Methyl violet and malachite green (10 ml) were then placed into two separate test tubes to which 2 mg of ZnO NPs were added. The test tubes were kept in the dark and incubated for an hour before being irradiated with sunlight [32, 33]. UV spectrum scans were taken in the range 200–800 nm every hour until complete degradation of the dye was achieved. Degradation percentage was calculated using the following formula:

$$\text{Degradation}(\%) = \frac{\text{OD control} - \text{OD sample}}{\text{OD control}} \times 100$$

MTT-Based Antiproliferative Assay

The cytotoxic effect of the synthesized ZnO NPs against human breast cancer cell lines was assessed by rapid colorimetric assay using 3-(4, 5-dimethylthiazol-2-yl)-2, 5-diphenyl tetrazolium bromide (MTT). The results were compared with those of untreated controls [34]. Screening experiments were performed as follows: the cells were seeded in 96-well plates in 100 μl of medium containing 5% fetal bovine serum (FBS) solution at a plating density of 10,000 cells/well. Well-plates were incubated at 37 °C, 5% CO₂ and 95% air, and 100% relative humidity 48 h prior to the addition of further compounds. After 48 h, compounds at various concentrations (10–1000 μg) were added and the well-plates were incubated at 37 °C, 5% CO₂ and 95% air, and 100% relative humidity for 48 h. Experiments were performed in triplicate and media prepared without the addition of samples were used as a control. After 48 h, 50 μl of MTT solution (5 mg/ml, dissolved in triple-distilled water) was added to each well before incubation at 37 °C for 4 h. The media were then removed and formed formazan crystals were dissolved in 100 μl of dimethyl sulfoxide (DMSO) and their absorbance was measured at 570 nm using a micro plate reader. Percentage cell inhibition was determined using the following formula [35]:

$$\text{Cell inhibition (\%)} = 100 - \frac{\text{Absorbance}(\text{Sample})}{\text{Absorbance}(\text{Control})} \times 100$$

Results and Discussion

Visual Characterization

Visual characterization is the first step in the confirmation of ZnO NP synthesis. The color of the particles changes on the addition of the leaf extract from a light brown to a whey-like color (yellowish white) as a precipitate forms (Fig. 1a). The reducing mechanism of artichoke leaf extract was given in the Fig. 1b. This method is supported by Santhoshkumar et al. [1], who reported that a color change from half white to pale yellow confirms the synthesis of ZnO NPs. Gnanasangeetha and Thambavani [36] also reported the appearance of a pale white precipitate following the green synthesis of ZnO NPs.

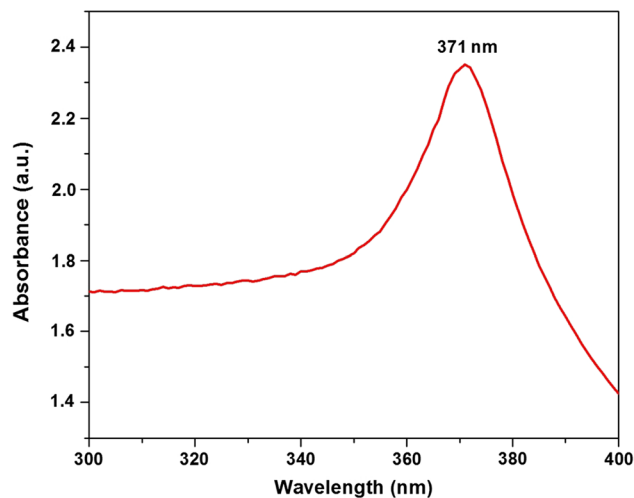


Fig. 2 UV spectrum of ZnO NPs

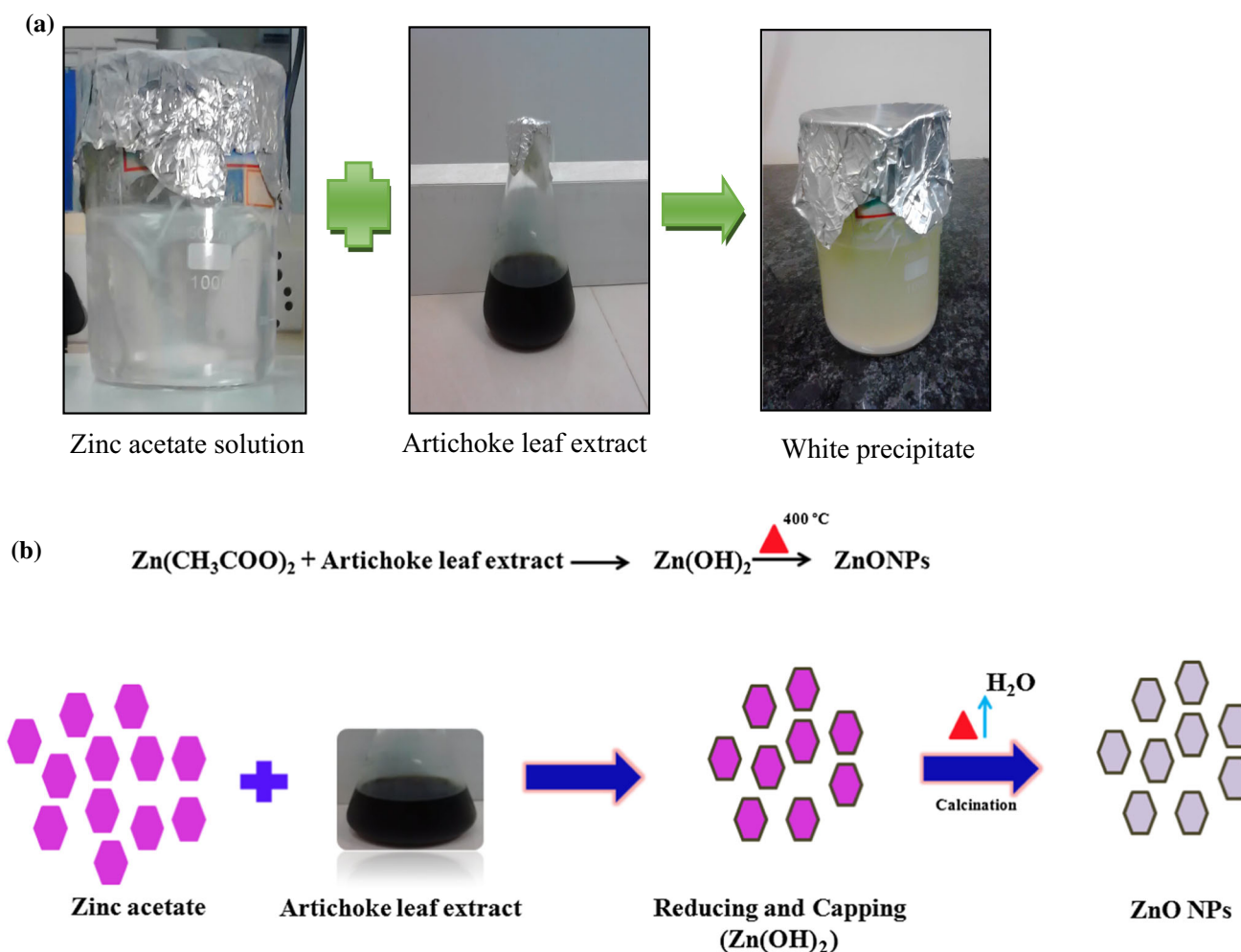
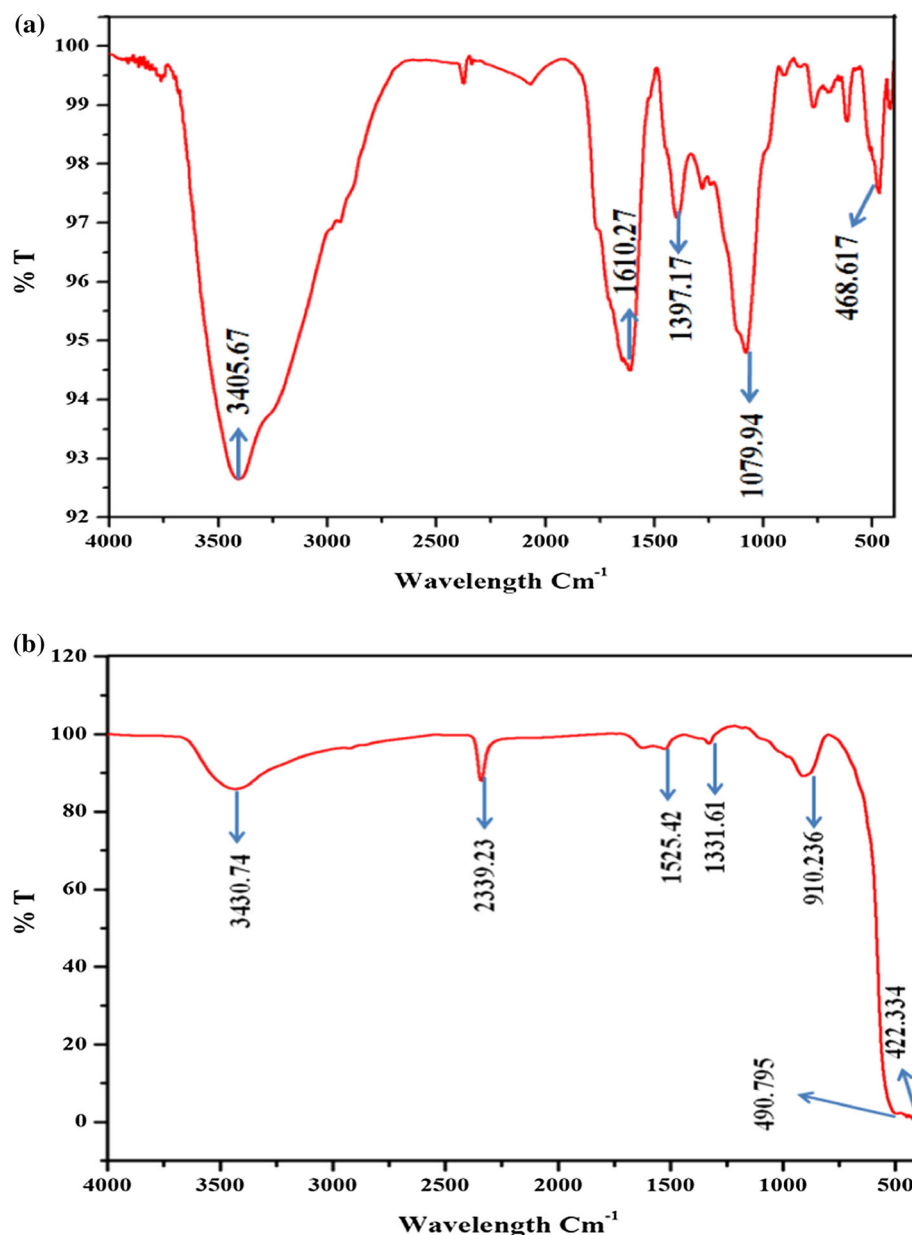


Fig. 1 a Color change and formation of white precipitate, b mechanism of reduction of ZnO NPs from zinc acetate by Artichoke leaves extract

Fig. 3 FT-IR spectra of artichoke leaf extract (a) and ZnO NPs (b)



UV Spectrophotometry

UV absorbance was determined by scanning at wavelengths between 250 and 400 nm. At a particular wavelength, the conducting electrons begin to oscillate as a result of surface plasmon resonance (SPR). As a result of SPR, a strong peak was observed at 371 nm (Fig. 2), which confirms the presence of ZnO NPs. Similar results were reported by Jamdagni et al. [15], Karthik et al. [37] and Suresh et al. [38], in which absorption peaks were observed at 369 nm, 374 nm, and 370 nm, respectively, corresponding to the characteristic range of ZnO NPs. Similarly, Al-Shabib et al. [39] reported the confirmation of ZnO NP synthesis based on the observation of an absorption peak at

385 nm in the visible UV spectra. Vennila and Jesurani [40] also reported that a peak at 390 nm corresponds to the presence of ZnO NPs, likely due to SPR.

FTIR

FTIR analysis was used to determine the role of functional groups and the involvement of biomolecules in the synthesis of ZnO NPs. Peaks were observed between the range of 400–4000 cm^{-1} . FTIR analysis of artichoke leaf extract showed a strong broad absorbance at 3405.67 cm^{-1} , characteristic of the (O–H) stretching frequency common to alcohol compounds. The peak at 1610.27 cm^{-1} corresponds to the (N–H) bending frequency common to

compounds containing an amine group. The peak at 1397.17 cm^{-1} is indicative of the (C-H) bending frequency characteristic of compounds containing an alkane group. The strong peak at 1079.94 cm^{-1} is indicative of the (C-O) stretching mode characteristic of alcohol compounds. A peak was also observed at 468.617 cm^{-1} (Fig. 3a). Concerning the spectra produced by the analysis of ZnO NPs (Fig. 3b), the strong and broad peak observed at 3430.74 cm^{-1} corresponds to an (O-H) bond and indicates the presence of an alcohol group. The very broad, strong peak at 2339.23 cm^{-1} is indicative of the (O-H) stretching frequency and suggests the presence of an acid. The peak at 1525.42 cm^{-1} (C=C) corresponds to the presence of an aromatic group. The weak peak at 1331.61 cm^{-1} is indicative of the (C-N) stretching frequency and suggests the presence of an amine group. The peak at 910.236 cm^{-1} is indicative of the ($=\text{C-H}$) bending frequency and its strong bands suggest the presence of an

alkene group. The peaks at 490.795 cm^{-1} and 422.334 cm^{-1} are characteristic of a (Zn-O) bond [8]. This result is supported by the findings of Vijayakumar et al. [8], in which peaks were observed between the range of $500\text{--}4000\text{ cm}^{-1}$ and a characteristic (Zn-O) stretching peak was observed at 413 cm^{-1} . Santhoshkumar et al. [1] also compared the spectra of nanoparticles and artichoke leaf extract and provided a similar interpretation.

SEM-EDXA

SEM was used to study the morphology of the ZnO NPs. The images showed spherically-shaped ZnO NPs ranging from 37 to 84 nm in size (Fig. 4a, b). The average particle size was 65.9 nm. Their elemental composition was studied using EDXA peaks (Fig. 4c), from which the composition was determined to be 80.17% Zinc and 19.83% oxygen. Santhoshkumar et al. [1] reported the morphology

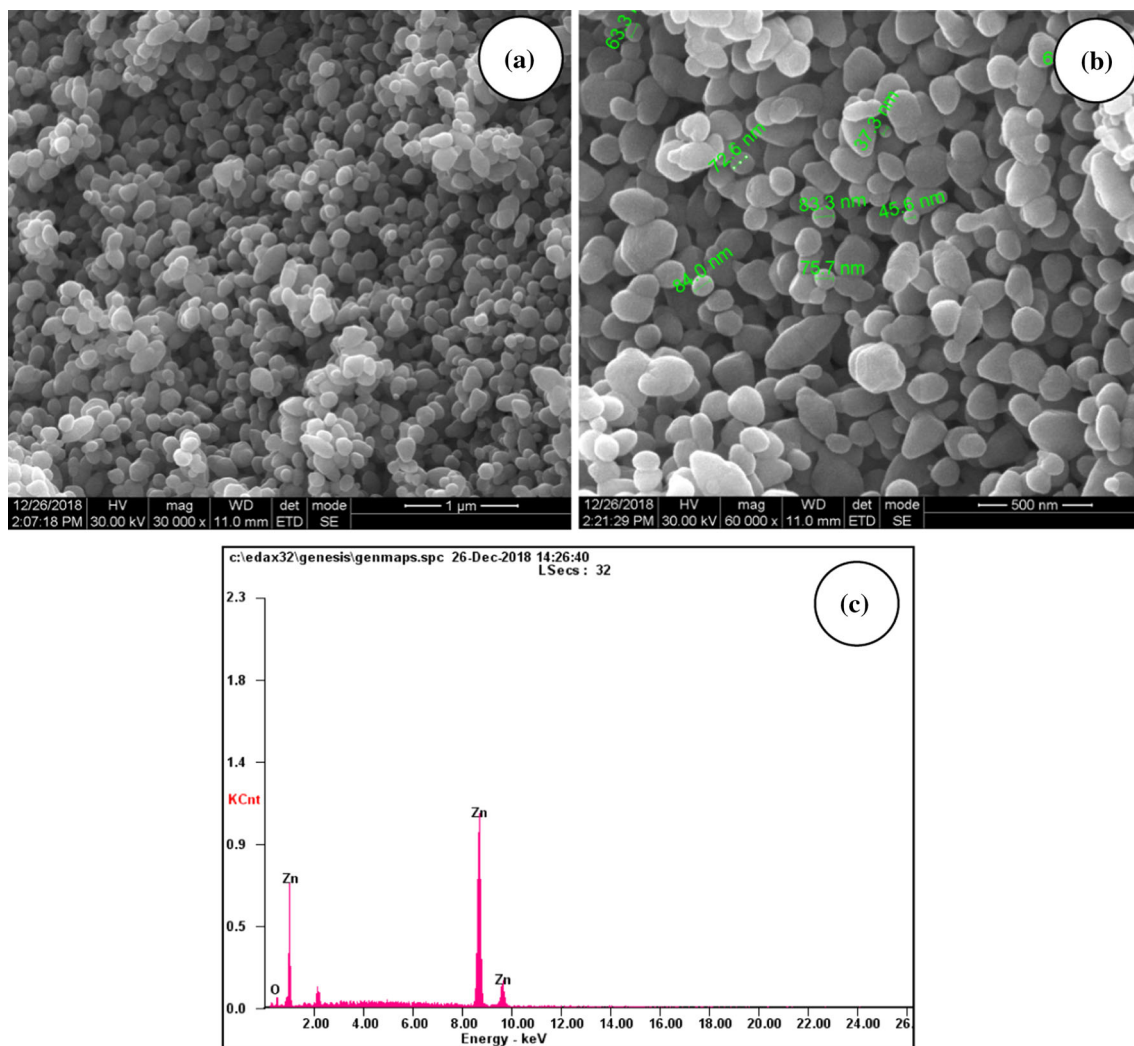


Fig. 4 Scanning electron microscopy images showing spherically-shaped ZnO NPs (**a** 30,000 \times ; **b** 60,000 \times ; **c** EDXA spectrum)

of spherical nanoparticles of particle size 70 nm using EDXA, finding the composition of the particles to be 75.36% zinc, 22.36% oxygen, and 2.29% carbon. Similarly, Ishwarya et al. [9] found an elemental composition of 78% zinc and 48% oxygen based on EDXA spectra. Datta et al. [41] reported quasi-spherically-, radially-, and cylindrically-shaped nanoparticles based on SEM images and reported an elemental composition of 97.6% zinc and 2.4% oxygen based on EDXA.

TEM-SAED

The size of the nanoparticles was analyzed through TEM analysis. The TEM image showed and confirmed that spherical shaped ZnO NPs and the size of the nanoparticles ranges between 20 and 70 nm (Fig. 5). The SAED pattern authenticates the crystalline nature of ZnO NPs. Our results were supported by Padalia and Chanda [42] who reported that spherical as well irregular shaped zinc oxide nanoparticles synthesized from *Ziziphus nummularia* leaf extract. Similarly, Patil and Taranath [43] also reported that *Limonia acidissima* L. leaf extract coated zinc oxide nanoparticles have spherical shape.

XRD Analysis

The structural properties and the crystalline size of ZnO NPs were studied using XRD analysis. Diffraction peaks were observed at 2θ 31.8°, 34.5°, 36.5°, 47.5°, 57°, 63°, 66.5°, 68°, 69.5°, 73°, 77°, 90°, 93°, 95.5°, and 98.5° (Fig. 6). These peaks were indexed as (100), (002), (101), (102), (110), (103), (200), (112), (201), (004), and (202) diffraction lattice planes, respectively. The crystalline size of the calcinated ZnO NPs was calculated using Debye–Scherrer’s formula:

$$D_p = (0.94 \times \lambda) / (\beta \times \cos\theta)$$

where D_p is the average crystalline size, β is the line broadening radians, θ is the Bragg’s angle, and λ is the X-ray wavelength (0.15418). The average crystalline size was found to be 20.5 nm. The crystalline nature and the size of the nanoparticles were studied using XRD. The nanoparticles’ crystalline nature was confirmed with reference to JCPDS file no. 89-7102. Their average size was calculated using Debye–Scherrer’s formula and found to be 20.5 nm. Vijayakumar et al. [8] reported the crystalline nature of ZnO NPs and reported an average size of 24 nm.

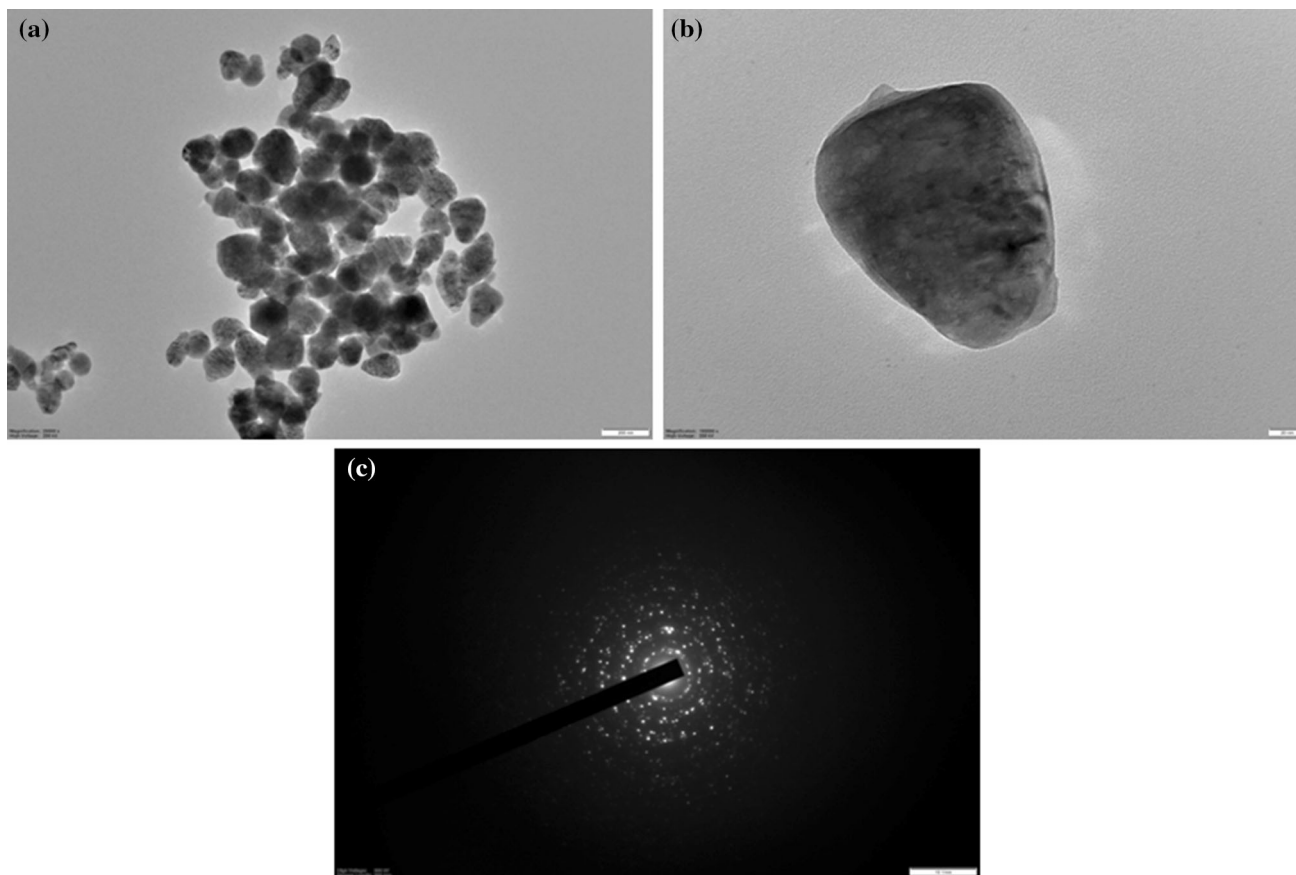


Fig. 5 Transmission electron microscopic images showing 200 nm (a), 20 nm (b) and SAED pattern (c) of ZnO NPs

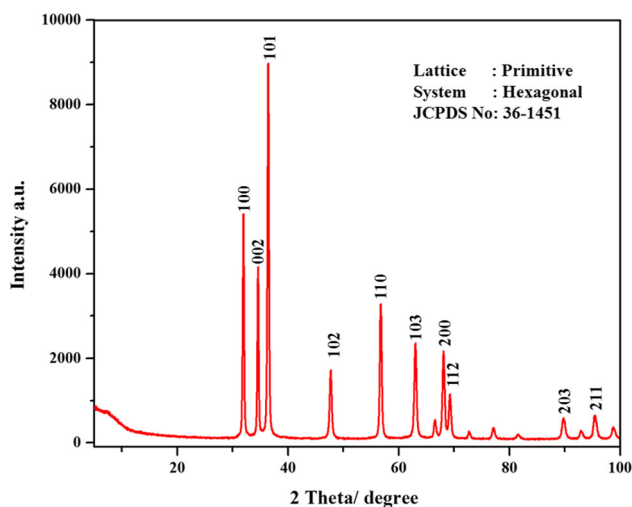


Fig. 6 XRD pattern showing the various Bragg's lattice planes of ZnO NPs

Ishwarya et al. [9] reported diffraction peaks and an average crystalline size of 5–15 nm.

Hemolytic Activity

The hemolytic activity of ZnO NPs was assessed to determine whether the synthesized nanoparticles destroyed the membrane of red blood cells, which can lead to the release of hemoglobin into the plasma (Fig. 7). We found that 100 $\mu\text{g/ml}$ of AT ZnO NPs exhibited 0.5% of total hemolytic activity and that there was no related destruction of red blood cells. Lower concentrations of nanoparticles were non-toxic and were found to be biocompatible. This assessment was crucial, as without it the use of ZnO NPs could result in dangerous pathological conditions. In the present study, 100 $\mu\text{g/ml}$ of ZnO NPs resulted in a hemolytic activity of 0.5%. Das et al. [27] Vinotha et al. and Abinaya et al. [44, 45] stated that hemolytic activity up to 5% is safe and a concentration of 2.5 mg/ml of ZnO NPs, when synthesized by direct thermal decomposition, can be used for their hemolytic activity. Muthukumarasamyvel

Fig. 7 Hemolytic activity assays using ZnO NPs



et al. [29] reported the results of hemolysis assays of dicationic amphiphiles using human erythrocytes.

Minimum Inhibitory Concentration

Micro broth dilution assays were used to identify the MIC_{50} using the synthesized AT ZnO NPs. For *S. aureus* (Gram-positive bacteria), the MIC_{50} was calculated as $> 0.7 \mu\text{g/ml}$. In *E. coli* (Gram-negative bacteria) inhibition was achieved at a concentration of 25 $\mu\text{g/ml}$, and in *P. aeruginosa* $> 100 \mu\text{g/ml}$ was required to induce an inhibitory effect. The minimum inhibitory concentration for fungal species, including *C. tropicalis*, was found to be 0.35 $\mu\text{g/ml}$. This was at odds to the result found for *C. albicans*, for which a concentration $> 100 \mu\text{g/ml}$ was required to produce inhibition (Table 1). Raju et al. [30] reported the MIC of nanostructured silver nanoparticles using *Enteromorpha intestinalis*. Jamdagni et al. [15] reported the MIC of green synthesized ZnO NPs using *Nyctanthes* leaf extract. *A. niger* had the lowest MIC_{50} value (16 $\mu\text{g/ml}$) and was determined to be sensitive to ZnO NPs. *Botrytis cineria* and *Penicillium expansum* had higher MIC_{50} values (128 $\mu\text{g/ml}$) relative to *A. niger*. The antibacterial activity of these nanoparticles could be due to their accumulation in the bacterial cell walls, which would alter their permeability, resulting in cell death. It has also been suggested that ZnO NPs produce reactive oxygen species, which induce cell death.

Photocatalytic Activity

Photocatalytic degradation activity was assayed using methyl violet. We observed 94.3% degradation in the dye following exposure to sunlight for 120 min (Fig. 8a), and malachite green exhibited 89.5% degradation after 120 min of exposure to sunlight (Fig. 8c). The rate constant of photocatalytic activity was calculated using Langmuir–Hinshelwood kinetic model. The rate constant of photocatalytic activity of ZnO NPs against methyl

Table 1 Minimum inhibitory concentration of ZnO NPs

S. No.	Species tested	MIC ₅₀ concentration (µg/ml)
Bacteria		
1.	<i>S. aureus</i> (ATCC 25923)	> 0.7
2.	<i>E.coli</i> (ATCC 25922)	25
3.	<i>P. aeruginosa</i> (ATCC 27853)	> 100
Fungi		
1.	<i>C. albicans</i> (IFM 40009)	> 100
2.	<i>C. tropicalis</i> (IFM 46521)	0.35

violet and malachite green was showed in Fig. 8b, d respectively. These results confirm the photocatalytic properties of ZnO NPs. A similar finding was reported by Raja et al. [32] using methylene blue. An absorption peak was observed at 660 nm and decreases in absorption were seen after 90 min of exposure to sunlight. Likewise, Karnan et al. [46] tested the photocatalytic activity of

ZnO NPs using methyl orange dye following exposure to UV light, reporting 83.99% decolorization effectiveness after 120 min of exposure. Similarly, Zheng et al. [47] found that ZnO nanoparticles synthesized using *Corymbia citriodora* leaf extract exhibited a photodegradative capacity of 83.45% and 59.47% using methylene blue after 90 min of UV irradiation.

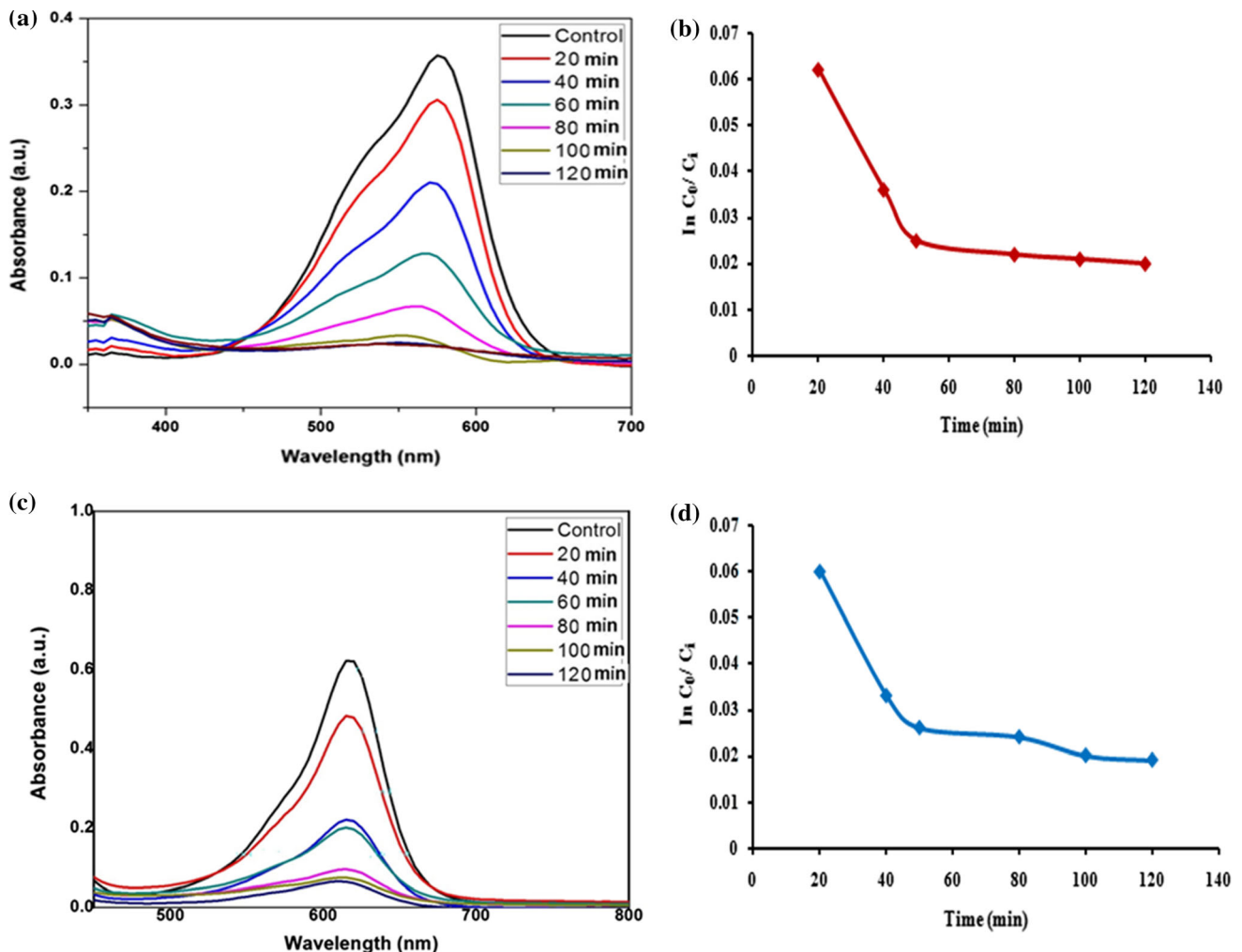
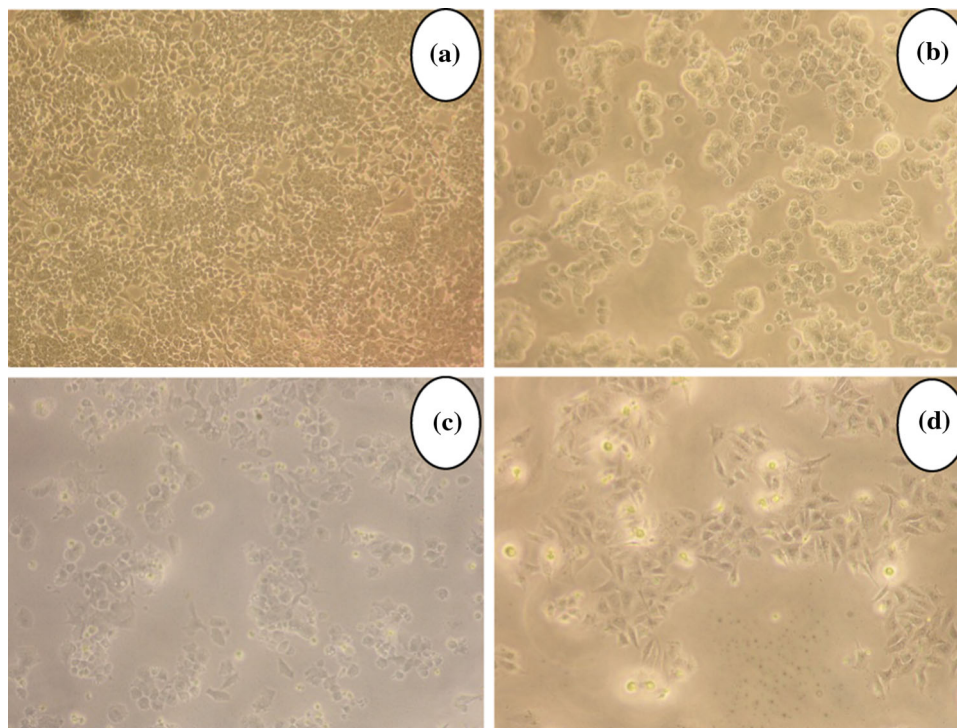


Fig. 8 Graph showing the photocatalysis of **a** methyl violet at 580 nm, **b** rate constant of ZnO NPs against methyl violet, **c** malachite green at 615 nm, **d** rate constant of ZnO NPs against malachite green

Fig. 9 Antiproliferative activity of ZnO NPs **a** MCF7 Control; **b** MCF7 Treated; **c** Vero Control; **d** Vero Treated)



MTT-Based Antiproliferative Assays

Antiproliferative assays were carried out using breast cancer cell line MCF-7 (Fig. 9a) and normal Vero cell lines (Fig. 9c). The following IC_{50} values were recorded: MCF 7: 65.31 $\mu\text{g}/\mu\text{l}$ ZnO NPs (Fig. 9b) and Vero: 957.85 $\mu\text{g}/\mu\text{l}$ ZnO NPs (Fig. 9d). Senthilkumar et al. [48] reported the results of in vitro cytotoxicity assays using ZnO NPs using *Tectona grandis* leaf extract. They reported IC_{50} values of 30.90 $\mu\text{g}/\text{ml}$ and 41.29 $\mu\text{g}/\text{ml}$ in the 5-Fluorouracil and MC3t3-E1 cell lines, respectively. Similarly, Mahendiran et al. [34] stated that the *Aloe vera* gel coated zinc oxide nanoparticles (ZnO-C) showed the highest anticancer activity against MCF-7, Hep-2, and HeLa cancer cell lines compared to other ZnO nanoparticles.

Conclusions

In the present study, spherically-shaped AT-ZnO NPs of diameter 65.9 nm were created. MIC_{50} assay results showed that bacterial strains are more susceptible to ZnO NPs compared to fungi. The photocatalytic degradation of methyl violet and malachite green was facilitated by ZnO NPs, providing evidence of their photocatalytic properties. Low concentrations of ZnO NPs exhibited only weak hemolytic activity and were found to be biocompatible in nature. Antiproliferative assays showed IC_{50} values of 65.31 $\mu\text{g}/\mu\text{l}$ and 957.85 $\mu\text{g}/\mu\text{l}$ using breast cancer cell line

MCF 7 and Vero cells, respectively. Thus, we conclude that ZnO NPs are safe for use in the development of novel treatment methods.

Acknowledgements The authors thank the Principal and the Management of Stella Maris College (Autonomous) Chennai for allowing them to use their research facilities. The second author thanks University Grants Commission Major Research Project (UGC MRP) (No. F.MRP-6994/16 (SERO/UGC) for financial support. SAIF IITM, Chennai and the CLRI-CATERS-CSIR-Central Leather Research Institute, Chennai are also acknowledged for allowing the authors to use their scanning electron microscopy (SEM) and FT-IR analysis facilities, respectively. The authors extend their appreciation to the Research Supporting Project number RSP-2019/70, King Saud University, Riyadh, Saudi Arabia. The authors thank the Deanship of Scientific Research and RSSU at King Saud University for their technical support.

Compliance with Ethical Standards

Conflict of interest The authors declare that they have no conflict of interest.

References

1. J. Santhoshkumar, S. V. Kumar, and S. Rajeshkumar (2017). *Resour. Eff. Technol.* **3**, 459–465.
2. M. Divya, B. Vaseeharan, M. Abinaya, S. Vijayakumar, M. Govindarajan, N. S. Alharbi, S. Kadaikunnan, J. M. Khaled, and G. Benelli (2018). *J. Photochem. Photobiol. B.* **178**, 211–218.
3. G. Bhumi and N. Savithamma (2014). *Int. J. Drug. Dev. Res.* **6**, 208–214.

4. P. Ramesh, A. Rajendran, and M. Meenakshisundaram (2014). *J. Nanosci. Nanotechnol.* **2**, 41–45.
5. V. Karthika, A. Arumugam, K. Gopinath, P. Kaleeswarran, M. Govindarajan, N. S. Alharbi, S. Kadaikunnan, J. M. Khaled, and G. Benelli (2017). *J. Photochem. Photobiol. B.* **167**, 189–199.
6. G. Benelli, F. Maggi, R. Pavela, K. Murugan, M. Govindarajan, B. Vaseeharan, R. Petrelli, L. Cappellacci, S. Kumar, A. Hofer, M. R. Youssefi, A. A. Alarfaj, J. S. Hwang, and A. Higuchi (2018). *Environ. Sci. Pollut. Res.* **25**, 10184–10206.
7. P. C. Nagajyothi, T. V. Sreekanth, C. O. Tettey, Y. I. Jun, and S. H. Mook (2014). *Bioorg. Med. Chem. Lett.* **24**, 4298–4303.
8. S. Vijayakumar, B. Vaseeharan, B. Malaikozhundan, and M. Shobiya (2016). *Biomed. Pharmacother.* **84**, 1213–1222.
9. R. Ishwarya, B. Vaseeharan, S. Kalyani, B. Banumathi, M. Govindarajan, N. S. Alharbi, S. Kadaikunnan, M. N. Al-anbr, J. M. Khaled, and G. Benelli (2018). *J. Photochem. Photobiol.* **178**, 249–258.
10. T. Singh, K. Jyoti, A. Patnaik, A. Singh, R. Chauhan, and S. S. Chandel (2017). *Genet. Eng. Biotechnol. J.* **15**, 31–39.
11. B. Banumathi, B. Vaseeharan, R. Ishwarya, M. Govindarajan, N. S. Alharbi, S. Kadaikunnan, J. M. Khaled, and G. Benelli (2017). *Parasitol. Res.* **116**, 1637–1651.
12. Y. I. Alivov, E. V. Kalinina, A. E. Cherenkov, D. C. Look, B. M. Ataev, A. K. Omaev, M. V. Chukichev, and D. M. Bagnall (2003). *Appl. Phys. Lett.* **83**, 4719–4721.
13. S. Vijayakumar, S. Mahadevan, P. Arulmozhi, S. Sriram, and P. K. Praseetha (2018). *Mat. Sci. Semicon. Proc.* **82**, 39–45.
14. B. Kumar, K. Smita, L. Cumbal, and A. Debut (2014). *Bioinorg. Chem. Appl.* **523869**, 1–7.
15. P. Jamdagni, P. Khatri, and J. S. Rana (2018). *JKSUS.* **30**, 168–175.
16. J. Fowsiya, G. Madhumitha, N. A. Al-Dhabi, and M. V. Arasu (2016). *J. Photochem. Photobiol.* **162**, 395–401.
17. R. Atchudan, T. N. Edison, S. Perumal, D. Karthikeyan, and Y. R. Lee (2016). *J. Photochem. Photobiol.* **162**, 500–510.
18. R. Atchudan, T. N. Edison, S. Perumal, N. Karthik, D. Karthikeyan, M. Shanmugam, and Y. R. Lee (2018). *J. Photochem. Photobiol. A Chem.* **350**, 75–85.
19. N. Muthuchamy, R. Atchudan, T. N. Edison, S. Perumal, and Y. R. Lee (2018). *J. Electroanal. Chem.* **816**, 195–204.
20. R. Atchudan, T. N. Edison, S. Perumal, M. Shanmugam, and Y. R. Lee (2017). *J. Photochem. Photobiol. A Chem.* **337**, 100–111.
21. O. Erdogan, M. Abbak, G. M. Demirbolat, F. Birtekocak, M. Aksel, S. Pasa, and O. Cevik (2019). *PLoS one.* **14**, (6), e0216496.
22. X. Zhu, H. Zhang, and R. Lo (2004). *J. Agric. Food Chem.* **52**, (24), 7272–7278.
23. M. A. Farag, S. H. El-Ahmady, F. S. Elian, and L. A. Wessjohann (2013). *Phytochemistry.* **95**, 177–187.
24. N. Tsevegsuren, G. Davaakhuu, and T. Udval (2014). *Mong. J. Chem.* **15**, 40–42.
25. R. Nateghi, F. Samadi, F. Ganji, and S. Zerehdaran (2013). *Int J Agric Sci.* **3**, (9), 678–688.
26. B. Malaikozhundan, B. Vaseeharan, S. Vijayakumar, K. Pandiselvi, M. A. Kalanjiam, K. Murugan, and G. Benelli (2017). *Microb. Pathog.* **104**, 268–277.
27. D. Das, B. C. Nath, P. Phukon, and S. K. Dolui (2013). *Colloids Surf. B.* **111**, 556–560.
28. A. Yildirim, E. Ozgur, and M. Bayindir (2013). *J. Mater. Chem. B.* **1**, 1909–1920.
29. T. Muthukumarasamyvel, R. Baskar, S. Chandirasekar, K. Umamaheswari, and N. Rajendiran (2016). *ACS Appl. Mater. Interfaces.* **8**, 25111–25126.
30. B. Raju, A. Muniyasamy, S. G. Prakash, A. S. Sundararaj, and U. Kesavachandran (2017). *J. Clust. Sci.* **28**, 1739–1748.
31. S. D. Sarker, L. Nahar, and Y. Kumarasamy (2007). *Methods.* **42**, 321–324.
32. A. Raja, S. Ashokkumar, R. P. Marthandam, J. Jayachandiran, C. P. Khatiwada, K. Kaviyarasu, R. G. Raman, and M. Swaminathan (2018). *J. Photochem. Photobiol.* **1**, (181), 53–58.
33. L. Fu and Z. Fu (2015). *Ceram. Int.* **41**, 2492–2496.
34. D. Mahendiran, G. Subash, D. A. Selvan, D. Rehana, R. S. Kumar, and A. K. Rahiman (2017). *BioNanoScience.* **7**, 530–545.
35. R. Balaji (2016). PhD Thesis, University of Madras, Chennai, India.
36. D. Gnanasangeetha and D. SaralaThambavani (2013). *Res. J. Mater. Sci.* **2320**, 6055.
37. S. Karthik, P. Siva, K. S. Balu, R. Suriyaprabha, V. Rajendran, and M. Maaza (2017). *Adv. Powder Technol.* **28**, 3184–3194.
38. D. Suresh, P. C. Nethravathi, H. Rajanaika, H. Nagabhushana, and S. C. Sharma (2015). *Mater. Sci. Semicond. Process.* **31**, 446–454.
39. N. A. Al-Shabib, F. M. Husain, I. Hassan, M. S. Khan, F. Ahmed, F. A. Qais, M. Oves, M. Rahman, R. A. Khan, A. Khan, and A. Hussain (2018). *J Nanomater.* **2018**, 14.
40. S. Vennila, S.S. Jesurani (2017). *Int. J. Chemtech. Res.* **10**, 271–275
41. A. Datta, C. Patra, H. Bharadwaj, S. Kaur, N. Dimri, and R. Khajuria (2017). *J Biotechnol Biomater.* **7**, 271–275.
42. H. Padalia and S. Chanda (2017). *Artif. Cells Nanomed. Biotechnol.* **45**, (8), 1751–1761.
43. B. N. Patil and T. C. Taranath (2016). *Int J Mycobact.* **5**, (2), 197–204.
44. V. Vinotha, A. Iswarya, R. Thaya, M. Govindarajan, N. S. Alharbi, S. Kadaikunnan, J. M. Khaled, M. N. Al-Anbr, and B. Vaseeharan (2019). *J Photochem Photobiol.* **25**, 111541.
45. M. Abinaya, B. Vaseeharan, M. Divya, A. Sharmili, M. Govindarajan, N. S. Alharbi, S. Kadaikunnan, J. M. Khaled, and G. Benelli (2018). *J. Trace Elem. Med. Biol.* **45**, 93–103.
46. T. Karnan and S. A. Selvakumar (2016). *J. Mol. Struct.* **1125**, 358–365.
47. Y. Zheng, L. Fu, F. Han, A. Wang, W. Cai, J. Yu, J. Yang, and F. Peng (2015). *Green Chem. Lett. Rev.* **8**, 59–63.
48. N. Senthilkumar, E. Nandhakumar, P. Priya, D. Soni, and M. Vimalan (2017). *New J. Chem.* **41**, 10347–10356.

Publisher's Note Springer Nature remains neutral with regard to jurisdictional claims in published maps and institutional affiliations.